Biosynthesized Silver Nanoparticles from *Glycosmis pentaphylla* (Retz.) DC.: A Multifunctional Nanomedicine for Antioxidant, Antidiabetic and Anticancer Therapeutics

Abdul Shafiulla[1], Mahanthesh Kumar G T[2], Ramesh C K*[1], Riaz Mahmood[3]

Abstract

Glycosmis pentaphylla (Retz.) DC., a medicinal plant widely distributed in tropical regions and traditionally used in Ayurveda and folk medicine, is known for its rich phytochemical profile comprising alkaloids, flavonoids, terpenoids, and phenolic compounds with reported antioxidant, antimicrobial, antidiabetic, and anticancer activities. Leveraging its bioactive constituents, the present study employed an eco-friendly green synthesis approach for the fabrication of silver nanoparticles (AgNPs) using *Glycosmis pentaphylla* bark extract as a natural reducing and stabilizing agent, followed by detailed physicochemical characterization and biological evaluation. The formation of AgNPs was confirmed by UV–visible spectroscopy through the appearance of a characteristic surface plasmon resonance band. Fourier-transform infrared (FTIR) analysis indicated the involvement of phenolic, hydroxyl, and amine functional groups in nanoparticle reduction and surface capping. Scanning electron microscopy (SEM) revealed nanoscale morphology with moderate aggregation, while X-ray diffraction (XRD) confirmed the crystalline face-centered cubic structure of metallic silver. Energy-dispersive X-ray (EDX) spectroscopy, particle size analysis (PSA), and zeta potential measurements further validated the elemental composition, nanoscale size distribution, and colloidal stability of the synthesized nanoparticles. Biological assessments demonstrated concentration-dependent antioxidant activity in DPPH and hydrogen peroxide scavenging assays. The AgNPs exhibited significant α-amylase inhibitory activity and enhanced glucose uptake, indicating promising antidiabetic potential. In vitro cytotoxicity studies revealed moderate yet selective antiproliferative effects against MDA-MB-231, A549, and KB-3-1 cancer cell lines, with comparatively lower toxicity toward normal L929 fibroblast cells. Additionally, the wound healing assay confirmed enhanced cell migration and wound closure following nanoparticle treatment. Overall, the findings highlight that *Glycosmis pentaphylla*-mediated AgNPs combine phytochemical functionality with nanoscale properties, resulting in multifunctional therapeutic potential. This study underscores the translational value of medicinal plant-based nanomaterials for future biomedical and nano pharmaceutical applications.

Graphical Abstract

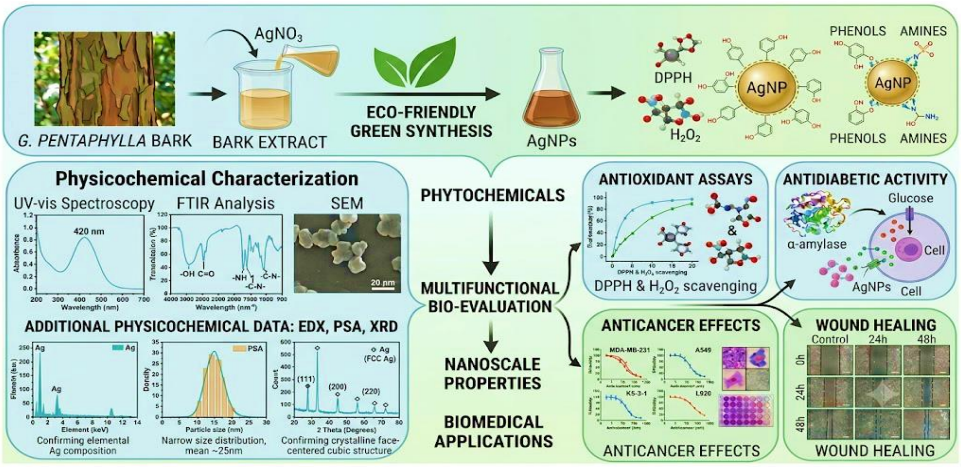

[1]Phytomedicine Laboratory, Department of Postgraduate Studies and Research in Biotechnology, Sahyadri Science College, Kuvempu University, Shivamogga Karnataka 577203

[2]Basic School of Sciences and Humanities, SR University, Warangal, Telangana, 506371, India

[3]Department of Postgraduate Studies and Research in Biotechnology and Bioinformatics, Jnana Sahyadri Shankaraghatta, Shivamogga Karnataka 577451

Corresponding Author*: Dr. Ramesh C. K. Phytomedicine Laboratory, Department of Postgraduate Studies and Research in Biotechnology, Sahyadri Science College, Kuvempu University, Shivamogga Karnataka 577203, E-mail: ckramck@gmail.com

Keywords: Green synthesis, silver nanoparticles, phytochemical-mediated reduction, antioxidant activity, Cytotoxicity, Wound healing, nanomedicine.

1. Introduction

Nanotechnology has emerged as a transformative interdisciplinary field with significant applications in medicine, pharmacology, and in the field of biotechnology. Among various nanomaterials, silver nanoparticles (AgNPs) have gained considerable attention owing to their unique physicochemical properties, including a high surface area-to-volume ratio, surface plasmon resonance, enhanced reactivity, and remarkable biological activities.[1,2] Traditionally, AgNPs are produced through physical and chemical techniques, but these methods often involve harmful chemicals, significant energy use, and pose environmental risks [3] As a result, green synthesis methods that employ biological materials have emerged as the favored option for the sustainable creation of metal nanoparticles.[4] The synthesis of nanoparticles using plants offers numerous benefits, such as being straightforward, cost-efficient, environmentally friendly, and utilizing the natural capping properties of plant constituents.[5,6] Bioactive compounds found in plant extracts, like flavonoids, phenolic acids, terpenoids, alkaloids, and proteins, serve as reducing and stabilizing agents in the formation of nanoparticles.[7,8] This reduction process driven by phytochemicals not only ensures compatibility with biological systems but may also improve the therapeutic potential of the nanoparticles produced.[9]

Glycosmis pentaphylla, a medicinal plant prevalent in tropical and subtropical areas, has been traditionally employed to address inflammation, fever, wounds, and disorders related to oxidative stress.[10] This plant is abundant in alkaloids, coumarins, flavonoids, and essential oils, all of which are known for their antioxidant and anti-inflammatory properties[11]. Although its pharmacological potential is well-recognized, there is a scarcity of studies on its use in nanobiotechnology for synthesizing silver nanoparticles[12]. In this study, silver nanoparticles were produced using the aqueous bark extract of Glycosmis pentaphylla through an environmentally friendly green method. The nanoparticles were thoroughly characterized using techniques such as UV-Visible spectroscopy, Scanning Electron Microscopy (SEM), X-ray Diffraction (XRD), Fourier-transform infrared spectroscopy (FTIR), Particle Size Analysis (PSA), and zeta potential analysis to evaluate their structural, morphological, and stability attributes. Additionally, in vitro pharmacological activities, including antioxidant (DPPH and H2O2 assays), antidiabetic (glucose uptake and alpha amylase activity), anticancer (MDAMB-231, A549, KB-3-1, and L929), and wound healing potential (scratch assay), were assessed to explore their biomedical applications. This research aims to establish a sustainable nanotechnology platform that combines phytochemistry and nanomedicine for potential therapeutic advancements.

2. Materials

All the chemicals and reagents utilized in this research were of analytical grade and were employed without any additional purification. Silver nitrate ($AgNO_3$), trisodium citrate, potassium dihydrogen phosphate (KH_2PO_4), sodium hydroxide (NaOH), hydrogen peroxide (30% H_2O_2), 2,2-diphenyl-1-picrylhydrazyl (DPPH), soluble starch, 3,5-dinitrosalicylic acid (DNSA), dimethyl sulfoxide (DMSO), glucose, and ethanol (99%) were sourced from commercial vendors. Porcine pancreatic α-amylase (1 U/mL), 3-(4, 5-dimethylthiazol-2-yl)-2, 5-diphenyltetrazolium bromide (MTT reagent), Dulbecco's Modified Eagle's Medium (DMEM), fetal bovine serum (FBS), trypsin–EDTA solution, antibiotic–antimycotic solution, phosphate-buffered saline (PBS), nutrient agar, nutrient broth, Sabouraud's dextrose agar, and Sabouraud's dextrose broth were acquired from HiMedia Laboratories (Mumbai, India) or similar suppliers. Ascorbic acid, Streptomycin, Fluconazole, Acarbose, Metformin, and Metronidazole served as reference standards for antioxidant, antimicrobial, and antidiabetic tests, respectively. The microbial strains Bacillus cereus (*NCIM* 2272), Escherichia coli (NCIM 1168), and Candida albicans (NCIM 1824) were obtained from the National Collection of Industrial Microorganisms (NCIM) in India. The cell lines used for cytotoxicity and migration experiments, including L929 mouse fibroblast cells, MDA-MB-231 human breast cancer cells, and A549 human lung cancer cells, were sourced from verified cell repositories. All culture plasticware, such as 96-well and 24-well plates, culture flasks, centrifuge tubes, and micropipette tips, were sterile and of tissue-culture grade. Double-distilled water was employed in all experiments. The instrumentation included a UV–visible spectrophotometer, microplate reader, CO_2 incubator (37°C, 5% CO_2), refrigerated centrifuge, laminar airflow cabinet, inverted phase-contrast microscope, magnetic stirrer with hot plate, analytical balance, pH meter, autoclave, and image analysis software for wound healing quantification.

3. Methodology

3.1. Preparation of Plant Extract

To synthesize nanoparticles, around 5 g of the plant extract was utilized. The extract underwent filtration using Whatman No. 1 filter paper to eliminate any solid particles and was then kept at 4°C for future use.

3.2. Green Synthesis of Silver Nanoparticles

Silver nanoparticles (AgNPs) were produced using a slightly modified version of the procedure outlined by Gudikandula and Maringanti (2016). In short, a 50 mL solution of 0.01 M aqueous silver nitrate ($AgNO_3$) was prepared under sterile conditions. To this solution, 5 g of plant extract was introduced, and the mixture was heated to a boil while being constantly stirred. Then, 5 mL of a 1% (w/v) trisodium citrate solution was gradually added to the mixture. The reaction was kept under continuous stirring and conducted in the dark to avoid the photoreduction of silver ions. A noticeable color shift from pale yellow to reddish-brown within an hour signified the formation of AgNPs, attributed to the surface plasmon resonance (SPR) phenomenon.[13,14]

3.3. Purification of Synthesized Nanoparticles

The reaction mixture was subjected to centrifugation at 10,000 rpm for 45 minutes to gather the synthesized nanoparticles as a pellet. This pellet was subsequently rinsed three to four times with deionized water to remove any unreacted silver ions and residual plant biomolecules. The purified nanoparticles were then re-suspended in deionized water and dried under controlled conditions for further analysis.[13,15]

3.4. Storage and Characterization

The Ag silver nanoparticles that were synthesized were kept in sealed containers in a cool, dry, and dark setting until they were ready for further analysis. Several analytical techniques were employed to confirm the physicochemical properties of the AgNPs [16]. The UV–Vi absorption spectra were captured using a Shimadzu UV-1800 spectrophotometer, spanning a wavelength range of 200–800 nm with quartz cuvettes.[17] Fourier-transform infrared (FTIR) spectroscopy was performed on a Thermo Nicolet 6700 instrument to detect potential functional groups, covering the range of 200-4000 cm^{-1}[18,19]. The crystalline structure of the AgNPs was assessed through X-ray diffraction (XRD) using a Shimadzu XRD-7000 model.[20] Scanning electron microscopy (SEM) was conducted with a JEOL JEM 2100 operating at 90 kV to investigate the surface morphology and particle size, supplemented by high-resolution SEM.[21] Energy-dispersive X-ray (EDX) analysis, carried out with a JEOL EDX model JSM-5610 LV, verified the presence of Ag and other elements. [22] The surface charge of the synthesized AgNPs was measured using a zeta potential analyzer (HORIBA Nanoparticle Analyzer, SZ100).[23]

3.5. Evaluation of the Pharmacological Potential of Synthesized AgNPs.

3.5.1. Evaluation *in vitro* antioxidant activity

3.5.1.1. DPPH Radical Scavenging Assay

The ability of the test samples to scavenge free radicals was assessed using the DPPH (2,2-diphenyl-1-picrylhydrazyl) assay, following the procedure outlined by Burits and Bucar, with minor adjustments. In summary, 1 mL of a freshly made DPPH solution (0.004% w/v in 99% ethanol) was combined with 3 mL of the test sample solution (100 µg/mL in ethanol). The resulting mixture was then left to incubate at room temperature in the dark for 20 minutes to avoid photodegradation of the DPPH radical. After the incubation period, the mixture was vortexed, and its absorbance was recorded at 517 nm using a UV–visible spectrophotometer, with 99% ethanol serving as a blank.[24] Ascorbic acid was employed as a reference standard under the same conditions. The percentage of DPPH radical scavenging activity was determined using the following formula:

$$\% \text{ Antioxidant activity} = [(Ac - As)/Ac] \times 100 \quad \text{--------- (1)}$$

where Ac and As are the absorbance values of the control and sample, respectively.

3.5.1.2. Hydrogen Peroxide Scavenging Assay

The hydrogen peroxide (H_2O_2) scavenging activity of the test compounds was assessed using a modified version of the method outlined by Ruch et al. (1989). To prepare the phosphate buffer at pH 7.4, 6.8 g of potassium dihydrogen phosphate (KH_2PO_4) and 1.5 g of sodium hydroxide (NaOH) were dissolved in 1000 mL of double-distilled water. A 40 mM hydrogen peroxide solution was created by mixing 4.420 mL of 30% H_2O_2 with 50 mL of the phosphate buffer (pH 7.4). This H_2O_2 solution was freshly prepared before each experiment and kept in a dark amber volumetric flask to avoid decomposition. For the assay, 3 mL of varying concentrations of the test compounds (dissolved in phosphate buffer) were combined with 0.5 mL of the 40 mM hydrogen peroxide solution and left to incubate for 10 minutes at room temperature. Following incubation, the absorbance was recorded at 230 nm using a UV–visible spectrophotometer, with a blank containing only hydrogen peroxide in phosphate buffer as a reference. [25]Ascorbic acid served as a positive control. All experiments were conducted in duplicate, and the mean values were noted. Each sample was tested in triplicate. The percentage of inhibition was determined using the appropriate formula.

$$\% \text{ Antioxidant activity} = [(Ac - As)/Ac] \times 100 \quad \text{--------- (2)}$$

Where, Ac and As are the absorbance values of the control and sample, respectively.

3.6. Evaluation *in vitro* antidiabetic activity

3.6.1. α-Amylase Inhibitory Assay

The inhibitory effect of the test samples on porcine pancreatic α-amylase was assessed using the 3,5-dinitrosalicylic acid (DNSA) method, as outlined by [26], with minor adjustments. In summary, 100 µL of test samples at different

concentrations and 100 µL of acarbose (a standard drug) were combined with 100 µL of α-amylase solution (1 U/mL) and 200 µL of 20 mM sodium phosphate buffer (pH 6.9). The reaction mixtures were pre-incubated at 25 °C for 10 minutes before proceeding. Then, 200 µL of 1% (w/v) soluble starch prepared in 20 mM sodium phosphate buffer (pH 6.9) was added to start the reaction, and the mixture was incubated at 25 °C for another 10 minutes. The reaction was stopped by adding 1 mL of dinitro salicylic acid reagent and heating the mixture in a boiling water bath for 5 minutes. After cooling to room temperature, the reaction mixture was diluted with distilled water at a 1:5 ratio, and the absorbance was measured at 540 nm using a UV–visible spectrophotometer. A control containing all the reagents except the test sample was maintained. The percentage inhibition of α-amylase activity was calculated using the formula: The enzyme inhibition efficiency was determined by applying the equation provided below (3), where Ac and As represent the absorbances of the control and sample, respectively.

$$\%\, \boldsymbol{of} \propto \boldsymbol{-amylose\ inhibition} = [(\boldsymbol{Ac} - \boldsymbol{As})/\boldsymbol{Ac}] \times \mathbf{100} \quad \textbf{(3)}$$

3.6.2. Glucose Uptake Assay in Yeast Cells

The glucose uptake assay in yeast cells was conducted following the method outlined by [27], with minor adjustments. In summary, a 1% (w/v) yeast cell suspension was created by soaking commercial baker's yeast in distilled water overnight at room temperature. This suspension was then centrifuged at 4200 rpm for 5 minutes, and the supernatant (10 mL) was diluted with 90 mL of distilled water to achieve a consistent yeast-cell suspension. Various concentrations of the test compounds were prepared and mixed with a glucose solution (500 ng/mL) at 37°C for 10 minutes, using fluconazole as the reference standard. The yeast suspension was subsequently added to the reaction mixture and incubated under the same conditions to promote glucose uptake. After incubation, 2 mL of 3,5-dinitrosalicylic acid (DNSA) reagent was introduced, and the mixture was incubated at 37°C for 60 minutes, followed by centrifugation at 3800 rpm for 5 minutes. The absorbance of the supernatant was measured at 520 nm using a UV–visible spectrophotometer. A control containing only the glucose solution without the test compound was maintained, and the blank absorbance was recorded. The percentage increase in glucose uptake was calculated using the following formula: The experiment was conducted in triplicate to ensure accuracy, where Abs sample is the absorbance of the test sample, and Abs control is the absorbance of the control reaction.

$$\%\, \boldsymbol{Glucose\ uptake} = \boldsymbol{Abs\ control} - \frac{\boldsymbol{Abs\ sample}}{\boldsymbol{Abs\ control}} \times \mathbf{100} \quad \textbf{(4)}$$

3.7. Evaluation *in vitro* anticancer activity

3.7.1. In Vitro Cytotoxicity Assay (MTT Assay)

The cytotoxic effects of the synthesized nanoparticles in vitro were assessed using the MTT assay. In summary, cells that had been cultured were trypsinized and placed into a 15 mL centrifuge tube, followed by centrifugation at 300 × g to form a cell pellet. The cell concentration was adjusted with Dulbecco's Modified Eagle's Medium (DMEM) so that 200 µL of the suspension contained about 1×10^4 cells. Then, 200 µL of this cell suspension was added to each well of a 96-well microtiter plate and incubated at 37°C in a humidified environment with 5% CO_2 for 24 hours to facilitate cell attachment. After this incubation period, the used medium was carefully removed and replaced with 200 µL of fresh medium containing varying concentrations of nanoparticles (20, 40, 60, 80, and 100 µg/mL) prepared from the stock solution. The plate was incubated again under the same conditions for another 24 hours. After treatment, the medium containing the drug was removed, and 100 µL of medium with MTT reagent (final concentration 0.5 mg/mL) was added to each well [28–30]. The plate was incubated at 37°C with 5% CO_2 for 3 hours to allow the formation of purple formazan crystals. The medium was then carefully removed without disturbing the crystals, and 100 µL of dimethyl sulfoxide (DMSO) was added to dissolve the formazan crystals. The plate was gently shaken to ensure the dye was completely solubilized. Absorbance was measured at 570 nm with a reference wavelength of 630 nm using a microplate reader. The percentage of cell growth inhibition was calculated after subtracting the background and blank values, and the IC_{50} value (the concentration needed to inhibit 50% of cell viability) was determined from the dose–response curve for the respective cell line.

3.8. Evaluation *in vitro* wound healing activity

3.8.1. In Vitro Wound Healing (Scratch) Assay

The ability of the test compounds to promote cell migration was assessed using an in vitro scratch (wound healing) assay. In summary, cultured cells were trypsinized and placed into a 5 mL centrifuge tube, then centrifuged at 300 × g to form a cell pellet. The cell concentration was adjusted with Dulbecco's Modified Eagle's medium (DMEM). About 100 µL of the cell suspension was added to each well of a 24-well plate containing 1 mL of DMEM, and the plate was incubated at 37°C in a humidified environment with 5% CO_2 for 24 hours to achieve a confluent monolayer (~100% confluence). Without replacing the medium, a straight scratch was carefully made across the center of each well using a sterile 200 µL pipette tip held perpendicular to the plate surface. The scratch width matched the outer diameter of the pipette tips [31,32]. Detached cells were removed by gently washing the wells twice with culture medium, followed by two washes with 1× phosphate-buffered saline (PBS) solution. Fresh medium was then added to the wells, and test compounds at specified concentrations were introduced to the respective wells in 1 mL of the complete medium. The plates were incubated at 37°C with 5% CO_2 for 24 hours. Images of the scratched areas were

taken immediately after scratching (0 h) and after 24 hours of incubation using an inverted microscope at 4× magnification. Wound width was measured and quantified using MagVision software after proper calibration. The rate of cell migration (Rm) was calculated using the following formula:

Rm = (Wi - Wt)/T
Rm - Rate of cell migration (µm/h)
Wi - Initial Wound width (µm)
Wt - Final Wound width (µm)

Percentage of Wound Closure= Initial wound diameter-Final diameter ÷ Initial diameter X 100

4. Results

Silver nanoparticles were synthesized using a green method with *Glycosmis pentaphylla* bark extract. The appearance of a brown color in the reaction mixture signified the conversion of Ag^{+} ions into Ag^{0} nanoparticles, a process confirmed by surface plasmon resonance (SPR), indicating successful nanoparticle formation. The phytochemicals in the bark extracts serve dual roles as reducing and stabilizing agents, thus eliminating the need for harmful chemical reducers. After centrifugation and washing, the dried nanoparticle residue represents purified Ag silver nanoparticles, which can then undergo further physicochemical characterization and biological assessment.

A **B**

Figure 1. Preparation and recovery of plant extract residue. *(A)* Crude extract under continuous magnetic stirring showing a homogeneous brown suspension during extraction. *(B)* Dried solid residue obtained after solvent evaporation, indicating the concentrated nanoparticle powder used for further analysis.

4.1. Physicochemical Characterization of Synthesized AgNPs

4.1.1. UV–Visible Spectroscopy

The initial confirmation of silver nanoparticle (AgNP) formation was achieved through UV–visible spectroscopy (Fig. A). The absorption spectrum revealed a distinctive surface plasmon resonance (SPR) peak around 280.4 nm, with an absorbance of 0.233, signifying the conversion of Ag^{+} ions into Ag^{0} nanoparticles. This unique absorption band confirmed the creation of nanoparticles and indicated the presence of nanoscale silver particles stabilized by phytoconstituents from the plant extract. The broadness of the absorption curve suggests the polydispersity of the synthesized nanoparticles.

4.1.2. Fourier Transform Infrared (FTIR) Analysis

FTIR analysis (Fig. B) was conducted to determine the functional groups that play a role in the reduction and stabilization of AgNPs. The spectrum reveals a significant broad peak at 3233.85 cm^{-1}, which is linked to the O–H stretching vibrations of phenolic or alcoholic groups. The peak at 1606.44 cm^{-1} is associated with C=O stretching or the amide I band, indicating the participation of proteins or polyphenolic compounds. The band at 1513.93 cm^{-1} signifies aromatic C=C stretching, while the peak at 1339.71 cm^{-1} is related to the C–N stretching of amines. The absorption band at 1031.76 cm^{-1} corresponds to the C–O stretching vibrations of alcohols or ethers. These functional

groups verify that the biomolecules in the bark extract function as reducing and capping agents during the synthesis of nanoparticles.

4.1.3. Energy Dispersive X-ray (EDX) Analysis

EDX analysis verified the elemental makeup of the synthesized nanoparticles. The spectrum revealed a distinct signal for silver (Ag), confirming the presence of elemental Ag. Alongside Ag, there were minor peaks for carbon (C), oxygen (O), sodium (Na), magnesium (Mg), sulfur (S), potassium (K), and calcium (Ca), likely originating from phytochemical residues and plant-derived biomolecules involved in nanoparticle capping. The prominent Ag peak indicated the successful biosynthesis of Ag silver nanoparticles with minimal impurities.

4.1.4. Morphological Analysis (SEM)

The morphology of the surface and the size of the particles of the synthesized Ag silver nanoparticles were analyzed using scanning electron microscopy (SEM) (Fig. D). Images captured at varying magnifications (3.00 KX and 20.00 KX) showed the development of nanosized particles with irregular shapes and some degree of agglomeration. At a higher magnification of 20.00 KX (scale bar 300 nm), individual nanoparticles were visible, with sizes approximately ranging from ~90–150 nm, confirming their nanoscale formation. The particles appeared to be clustered, likely due to strong interparticle forces and phytochemical-mediated capping during the green synthesis process. The surface texture seemed relatively rough, indicating the presence of biomolecular coatings that provided stability to the nanoparticles.

4.1.5. X-ray Diffraction (XRD) Analysis

The crystalline structure of the synthesized AgNPs was verified through X-ray diffraction analysis (Fig. E). The XRD pattern displayed distinct and strong diffraction peaks at around 2θ values of 38°, 44°, 64°, and 77°, which correspond to the (111), (200), (220), and (311) crystallographic planes of face-centered cubic (fcc) silver, respectively. These characteristic Bragg reflections confirmed the formation of crystalline metallic silver nanoparticles. The sharp and well-defined peaks indicate the high crystallinity of the synthesized particles. Minor additional peaks observed in the diffractogram may be due to phytochemical residues associated with the capping of nanoparticles.

4.1.6. Particle Size Analysis (PSA)

The particle size distribution of the synthesized AgNPs was assessed through dynamic light scattering (DLS) (Fig. F). The histogram of size distribution displayed a relatively narrow pattern, with the majority of particles residing within the nanoscale range. The average hydrodynamic diameter was found to be approximately between ~80–150 nm, indicating successful synthesis at the nanoscale. The cumulative percentage curve demonstrated that most particles were under 200 nm, confirming a largely uniform size distribution. The slightly wider distribution could be due to minor aggregation in the aqueous suspension, a common occurrence in green-synthesized nanoparticles because of biomolecular capping layers. Overall, PSA and zeta potential analyses verified that the synthesized Ag silver nanoparticles were nanosized, moderately monodispersed, and colloidally stable, affirming their potential for biomedical applications.

4.1.7. Zeta Potential Analysis

Zeta potential analysis was employed to assess the surface charge and colloidal stability of the synthesized silver nanoparticles (AgNPs) (Fig. G). The zeta potential distribution curve showed a single distinct peak, which suggests a fairly uniform distribution of surface charge. The nanoparticles demonstrated a moderately high zeta potential value, as indicated by the peak distribution, which implies effective electrostatic stabilization within the suspension. The surface charge is likely influenced by negatively charged functional groups from plant phytoconstituents, which help prevent excessive aggregation through electrostatic repulsion. These findings suggest that the biosynthesized AgNPs have significant colloidal stability.

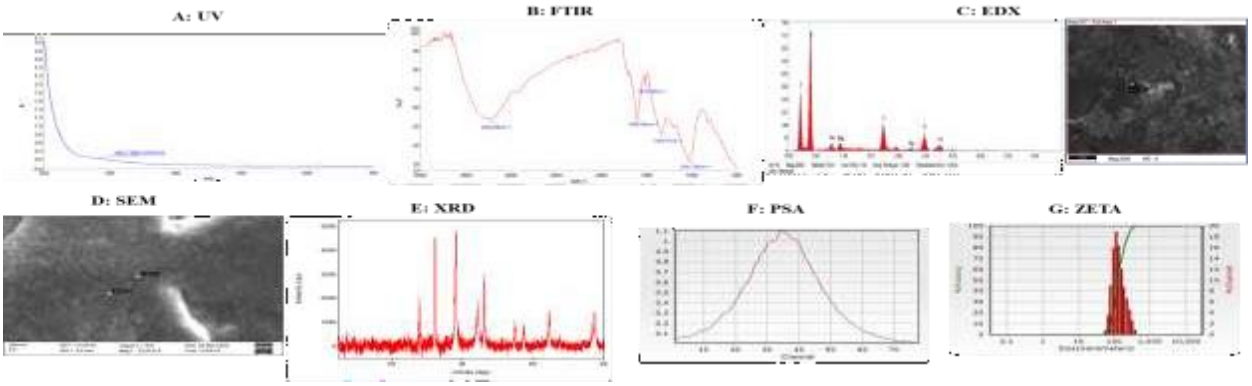

Fig. 2. Physicochemical characterization of biosynthesized silver nanoparticles (AgNPs). (A) UV–visible absorption spectrum showing the characteristic surface plasmon resonance (SPR) peak, confirming nanoparticle formation. (B) FTIR spectrum indicating the presence of functional groups (O–H, C=O, C=C, C–N, and C–O) involved in the

reduction and stabilization of AgNPs by the plant-derived biomolecules. (C) EDX spectrum confirming the elemental composition with a prominent silver (Ag) signal and minor peaks corresponding to phytochemical residues. (D) SEM micrograph illustrating the surface morphology and particle distribution, revealing irregular and aggregated nanosized particles. (E) XRD pattern displaying distinct diffraction peaks corresponding to the face-centered cubic (fcc) crystalline structure of metallic Ag. (F) Particle size analysis (PSA/DLS) showing the hydrodynamic diameter distribution within the nanoscale range. (G) Zeta potential distribution curve indicating the surface charge and colloidal stability of the nanoparticles.

4.2. Evaluation of the Pharmacological Potential of Synthesized AgNPs.

4.2.1. Evaluation *in vitro* antioxidant activity

4.2.1.1. DPPH Radical Scavenging Activity of Sliver nanoparticle

The antioxidant capabilities of the synthesized nanoparticles were assessed through the DPPH free radical scavenging assay and compared to the standard antioxidant, ascorbic acid. Both the nanoparticles and the standard showed an increase in radical scavenging activity that was dependent on concentration, ranging from 20 to 100 µg/mL. The nanoparticles achieved inhibition rates of 36.20 ± 0.002%, 42.21 ± 0.001%, 50.65 ± 0.001%, 56.27 ± 0.002%, and 64.13 ± 0.001% at concentrations of 20, 40, 60, 80, and 100 µg/mL, respectively. In contrast, ascorbic acid exhibited significantly higher inhibition rates of 46.85 ± 0.001%, 76.33 ± 0.001%, 85.40 ± 0.005%, 88.60 ± 0.001%, and 89.47 ± 0.003% at the same concentrations. Notably, the nanoparticles reached around 50% inhibition at 60 µg/mL, indicating moderate antioxidant activity, while the standard achieved over 76% inhibition at 40 µg/mL. Although the nanoparticles' radical-scavenging efficiency was lower than that of ascorbic acid, their dose-dependent activity confirmed a notable antioxidant potential, likely due to bioactive phytoconstituents serving as reducing and stabilizing agents during the synthesis of the nanoparticles.

Table 1. Comparative DPPH Radical Scavenging Activity of Ascorbic Acid and Synthesized Nanoparticles

Concentration (µg/mL)	**Ascorbic Acid % Inhibition**	**Nanoparticles % Inhibition**
20	46.85±0.001	36.20±0.002
40	76.33±0.001	42.21±0.001
60	85.40±0.005	50.65±0.001
80	88.60±0.001	56.27±0.002
100	89.47±0.003	64.13±0.001

4.2.1.2. Hydrogen Peroxide (H_2O_2) Scavenging Activity

The hydrogen peroxide scavenging capability of the synthesized nanoparticles was tested and compared to that of the standard antioxidant, ascorbic acid, over a concentration range of 20–100 µg/mL. Both the standard and the nanoparticles demonstrated a concentration-dependent increase in their ability to scavenge H_2O_2. Ascorbic acid showed inhibition percentages of 14.55 ± 0.001%, 21.82 ± 0.002%, 31.82 ± 0.001%, 58.18 ± 0.003%, and 64.55 ± 0.001% at concentrations of 20, 40, 60, 80, and 100 µg/mL, respectively. Similarly, the synthesized nanoparticles exhibited inhibition rates of 12.46 ± 0.001%, 13.61 ± 0.006%, 21.64 ± 0.002%, 46.23 ± 0.001%, and 53.55 ± 0.003% at the same concentrations. A marked increase in scavenging activity was observed at higher concentrations (80 and 100 µg/mL) for both samples. Although the nanoparticles consistently showed lower scavenging efficiency compared to ascorbic acid at all tested concentrations, the results highlight a significant potential for neutralizing hydrogen peroxide. This activity suggests that bioactive phytochemicals on the nanoparticle surface may enhance their antioxidant properties by converting hydrogen peroxide into water and oxygen.

Table 2. The hydrogen peroxide (H_2O_2) scavenging activity of the synthesized nanoparticles and standard ascorbic acid was evaluated at different concentrations (20–100 µg/mL). Values are expressed as mean ± standard deviation (n = 2).

Concentration (µg/mL)	**Ascorbic Acid % Inhibition**	**Nanoparticles % Inhibition**
20	14.55±0.001	12.46±0.001
40	21.82±0.002	13.61±0.006
60	31.82±0.001	21.64±0.002
80	58.18±0.003	46.23±0.001
100	64.55±0.001	53.55±0.003

4.3. Evaluation of *in vitro* antidiabetic activity

4.3.1. α-Amylase Inhibitory Activity

The synthesized nanoparticles' ability to inhibit α-amylase was assessed at concentrations between 20 and 100 µg/mL and compared to the standard drug, Acarbose. Both the standard and the nanoparticles exhibited strong enzyme-inhibitory effects at all tested levels. The standard drug showed high inhibition rates of 92.44%, 92.90%, 93.19%, 94.14%, and 96.97% at 20, 40, 60, 80, and 100 µg/mL, respectively. Similarly, the nanoparticles demonstrated significant inhibitory activity, with inhibition percentages of 77.90%, 81.49%, 82.74%, 84.07%, and 86.61% at the same concentrations. An increase in enzyme inhibition was noted with higher concentrations for both samples, indicating a dose-dependent effect. Although the nanoparticles' inhibitory effect was slightly less than that of the standard drug, the findings revealed a notable potential for α-amylase inhibition. The high inhibition levels suggest that the synthesized nanoparticles could effectively disrupt carbohydrate hydrolysis, highlighting their potential antidiabetic properties.

Table 3. α-Amylase inhibitory activity of the synthesized nanoparticles and standard (acarbose) at different concentrations (20–100 µg/mL). Values represent the percentage inhibition of enzyme activity.

Concentration (µg/mL)	Standard % Inhibition	Nanoparticle % Inhibition
20	92.44±0.001	77.90±0.001
40	92.90±0.002	81.49±0.002
60	93.19±0.001	82.74±0.002
80	94.14±0.001	84.07±0.001
100	96.97±0.003	86.61±0.001

4.3.2. Glucose Uptake Assay in Yeast Cells

The influence of synthesized nanoparticles on glucose uptake was investigated in yeast cells and compared to the standard drug, metronidazole, over a concentration range of 20 to 100 µg/mL. Both the standard drug and the nanoparticles demonstrated a concentration-dependent increase in glucose uptake activity. Metronidazole showed percentage increases of 40.65%, 59.61%, 66.28%, 74.36%, and 78.88% at concentrations of 20, 40, 60, 80, and 100 µg/mL, respectively. Conversely, the synthesized nanoparticles exhibited glucose uptake enhancements of 13.79%, 16.47%, 27.24%, 41.52%, and 49.89% at the same concentrations. A consistent rise in glucose uptake was observed with increasing nanoparticle concentrations, achieving nearly 50% enhancement at 100 µg/mL. Although the nanoparticles' activity was consistently lower than that of the standard drug across all tested concentrations, the results highlighted a significant potential for glucose uptake. This indicates that the nanoparticles could assist in cellular glucose transport, underscoring their potential application in antidiabetic therapy.

Table 4. Effect of synthesized nanoparticles and standard (metronidazole) on glucose uptake in yeast cells at different concentrations (20–100 µg/mL). Values represent the percentage increase in glucose uptake.

Concentration (µg/mL)	Std- Metronidazole % Inhibition	Nanoparticle% Inhibition
20	40.65±0.001	13.79±0.006
40	59.61±0.005	16.47±0.001
60	66.28±0.003	27.24±0.002
80	74.36±0.001	41.52±0.001
100	78.88±0.007	49.89±0.003

4.4. Evaluation of the *in vitro* Anticancer Potential of Synthesized AgNPs.

4.4.1. In Vitro Cytotoxic Activity (MTT Assay)

The cytotoxic effects of the synthesized silver nanoparticles (AgNPs) were assessed on human cancer cell lines and a normal fibroblast cell line using the MTT assay after 24 hours of exposure. The IC_{50} values were derived from the dose–response curves. The AgNPs demonstrated notable cytotoxicity against all the cancer cell lines tested. Among these, KB-3-1 cells were the most sensitive, with an IC_{50} value of 59.77 µg/mL, followed by MDA-MB-231 (62.82 µg/mL) and A549 (69.11 µg/mL) cells. Conversely, the normal L929 fibroblast cell line showed a relatively higher IC_{50} value of 79.56 µg/mL, indicating reduced sensitivity to the nanoparticles. The lower IC_{50} values observed in cancer cell lines compared to the normal cell line suggest that the synthesized AgNPs exhibit selective cytotoxicity towards cancerous cells. These results suggest that the nanoparticles have promising anticancer potential, especially against breast and oral carcinoma cell lines.

Table 5. IC_{50} Values of Synthesized AgNPs Against Different Cell Lines (24 h Treatment)

Sample	Cell Line	IC_{50} (µg/mL) – 24 h
AgNPs	MDA-MB-231	62.82

	A549	69.11
	KB-3-1	59.77
	L929	79.56

4.5. Evaluation of the *in vitro* Wound Healing Potential of Synthesized AgNPs.

4.5.1. In Vitro Cell Migration and Wound Healing Assay

The impact of AgNPs on cell migration was assessed through the scratch wound healing assay at intervals of 12 and 24 hours, and the results were compared to both an untreated control and a standard treatment (5 µg). The control group without treatment showed minimal cell movement, with measurements of 2.89 µm at 12 hours and 4.24 µm at 24 hours. Conversely, the standard treatment resulted in significantly increased migration, recording 24.21 µm at 12 hours and 16.11 µm at 24 hours. The group treated with AgNPs at the IC_{50} concentration displayed moderate migration, with 10.21 µm at 12 hours and 8.77 µm at 24 hours. Similarly, the analysis of percentage wound closure indicated that untreated cells achieved only 7.88% closure at 12 hours and 21.45% at 24 hours. The standard treatment showed a much higher wound closure rate of 54.66% at 12 hours and 94.19% at 24 hours. The AgNP-treated group achieved 27.34% wound closure at 12 hours and 75.54% at 24 hours post-treatment. These findings suggest that AgNPs significantly improved cell migration and wound closure compared to untreated cells, especially at the 24-hour mark. Although their effectiveness was less than that of the standard treatment, the nanoparticles exhibited notable wound-healing potential, indicating their potential role in enhancing cellular migration and tissue regeneration.

Table 6. Effect of AgNPs on Cell Migration and Wound Closure at 12 h and 24 h

Treatments	**Dose (µg)**	**Cell Migration (µm) – 12 h**	**Cell Migration (µm) – 24 h**	**Wound Closure (%) – 12 h**	**Wound Closure (%) – 24 h**
Untreated	0	2.89	4.24	7.88	21.45
Standard	5	24.21	16.11	54.66	94.19
AgNPs	IC_{50}	10.21	8.77	27.34	75.54

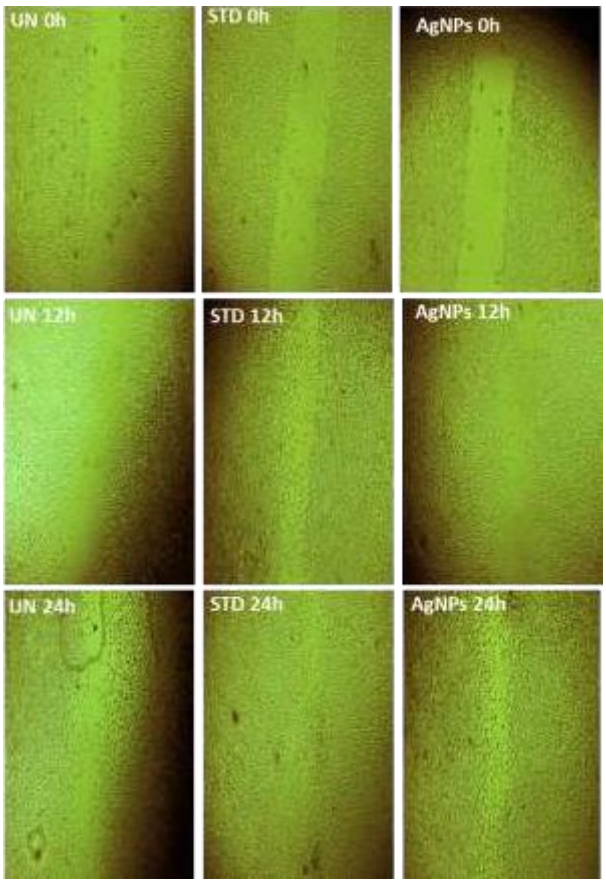

Fig. 2. Representative micrographs of the scratch wound healing assay showing cell migration at 0, 12, and 24 h under different treatments. Untreated control (UN), standard drug (STD), and silver nanoparticle (AgNP)-treated groups are shown at the respective time intervals. At 0 h, a clear wound gap was visible in all groups. Progressive closure of the scratched area was observed over time, with minimal migration in the untreated group, marked wound closure in the standard-treated group, and moderate but significant migration in the AgNP-treated group at 12 and 24 h. The images

demonstrate the time-dependent enhancement of cell migration and wound closure following AgNP treatment compared to the untreated control.

5. Discussion

The current study illustrates the effective green synthesis of silver nanoparticles (AgNPs) through the use of plant bark extract, emphasizing their versatile potential. This biosynthetic method offers an environmentally friendly and sustainable alternative to traditional chemical techniques, employing phytochemicals as both reducing and stabilizing agents. The observed color change and the specific UV–visible absorption band confirmed the creation of AgNPs, attributed to surface plasmon resonance (SPR), a unique optical characteristic of metallic silver nanoparticles.[33,34]FTIR analysis identified the presence of hydroxyl, carbonyl, aromatic, and amine functional groups, suggesting the involvement of polyphenols, proteins, and other secondary metabolites in the reduction and capping processes[35]. These biomolecules likely aid in stabilizing the nanoparticles and enhancing their biological activity. SEM images showed nanosized particles with irregular shapes and moderate aggregation, a common feature in green-synthesized nanoparticles due to biomolecular surface interactions. XRD analysis verified the crystalline nature of the AgNPs, with diffraction peaks matching the face-centered cubic (fcc) structure of metallic silver, further confirming successful synthesis. EDX results supported the elemental purity of silver with minimal extraneous signals, while zeta potential and particle size analyses indicated nanoscale distribution and adequate colloidal stability, crucial for biomedical applications.[36,37]Biological assessment showed that the synthesized AgNPs exhibited notable antioxidant activity, demonstrated by the concentration-dependent scavenging of DPPH and hydrogen peroxide radicals. Although their activity was lower than that of standard ascorbic acid, the nanoparticles showed significant free radical neutralization. This effect may be due to phytochemical residues on the nanoparticle surface, which enhance electron-donating capacity and contribute synergistically to antioxidant behavior[38]. The ability to scavenge reactive oxygen species is particularly important for alleviating oxidative stress-related disorders. The α-amylase inhibitory assay showed significant enzyme inhibition that increased with dosage, suggesting potential antidiabetic effects by hindering carbohydrate digestion and glucose release. Supporting this, the glucose uptake assay in yeast cells indicated that the nanoparticles boosted glucose utilization as concentrations rose[39]. These findings imply that the synthesized AgNPs might regulate blood sugar through two mechanisms: enzyme inhibition and enhanced glucose uptake. Cytotoxicity studies demonstrated moderate yet notable antiproliferative effects on MDA-MB-231, A549, and KB-3-1 cancer cells, while showing relatively lower toxicity towards normal L929 fibroblasts. The lower IC_{50} values in cancer cells indicate a level of selectivity, a desirable trait in anticancer treatments[40,41]. The cytotoxic action of AgNPs is often linked to the generation of reactive oxygen species, mitochondrial dysfunction, membrane damage, and apoptosis induction, which could explain the observed antiproliferative effects. Additionally, the wound healing assay showed improved cell migration and wound closure in AgNP-treated groups compared to untreated controls.[42,43] Although the activity was less than that of the standard treatment, the significant improvement at 24 hours suggests that AgNPs could enhance cellular migration and tissue regeneration. This effect might be related to the modulation of cellular signaling pathways involved in proliferation and migration. Overall, the combined physicochemical characterization and biological results indicate that green-synthesized AgNPs have multifunctional therapeutic properties, including antioxidant, antidiabetic, anticancer, and wound-healing activities[44,45]. The phytochemical capping not only stabilizes the nanoparticles but may also boost their bioactivity through synergistic interactions with the phytochemicals. These findings support the potential use of biosynthesized AgNPs as promising candidates for further preclinical development in nanomedicine.[2,46]

6. Conclusion

In this study, silver nanoparticles (AgNPs) were synthesized using a green and sustainable method, employing plant bark extract as a natural reducing and stabilizing agent. The biosynthesis was confirmed through UV–visible spectroscopy, while FTIR analysis indicated the involvement of phytoconstituents in nanoparticle reduction and surface capping. SEM analysis revealed nanoscale morphology with moderate aggregation, and XRD confirmed the crystalline face-centered cubic structure of Ag. EDX, particle size analysis, and zeta potential measurements further validated the elemental composition, nanoscale distribution, and colloidal stability of the synthesized nanoparticles. Biological evaluations demonstrated that the biosynthesized AgNPs possess significant multifunctional properties. The nanoparticles exhibited concentration-dependent antioxidant activity in both the DPPH and hydrogen peroxide scavenging assays. Substantial α-amylase inhibitory activity and enhanced glucose uptake in yeast cells indicate promising antidiabetic potential. In vitro cytotoxicity studies revealed selective antiproliferative activity against cancer cell lines, with comparatively lower toxicity toward normal fibroblast cells. Furthermore, the wound-healing assay confirmed enhanced cell migration and wound closure following AgNP treatment, supporting their potential role in tissue regeneration. Collectively, these findings establish that plant-mediated AgNPs combine structural stability with broad-spectrum biological activity, highlighting their potential as multifunctional nanotherapeutic agents. Further mechanistic investigations and in vivo studies are warranted to elucidate the molecular pathways and advance their translational applications in nanomedicine.

Author Contributions: RCK and AS designed the study and; AS Performed experiments. RCK GTM and AS analyzed the data. Surveying and altering MGT and RM. RCK and AS data interpretation and manuscript writing. All the authors have read and agreed to the published version of the manuscript.

Declarations

Ethics approval and consent to participate: Not required.

Funding: This research received no external funding

Data availability: The datasets used and analyzed during the current study are available from the corresponding author on request.

Plant Guidelines: The authors confirm that the use of plants in the present study complies with international, national and/or institutional guidelines.

Competing interests: The authors declare no competing interests.

References

[1] F. Eker, E. Akdaşçi, H. Duman, M. Bechelany, S. Karav, Green Synthesis of Silver Nanoparticles Using Plant Extracts: A Comprehensive Review of Physicochemical Properties and Multifunctional Applications, IJMS 26 (2025) 6222. https://doi.org/10.3390/ijms26136222.

[2] K. Selvam, A. Ragu Prasath, A.K. Alanazi, A Review of Recent Developments in Green Synthesis of Silver Nanoparticles: Antioxidant and Antibacterial Applications., Microscopy Res &Amp; Technique 89 (2025) 134–147. https://doi.org/10.1002/jemt.70060.

[3] A.-R. Phull, Q. Abbas, A. Ali, H. Raza, S.J. Kim, M. Zia, I.-U. Haq, Antioxidant, cytotoxic and antimicrobial activities of green synthesized silver nanoparticles from crude extract of Bergenia ciliata, Future Journal of Pharmaceutical Sciences 2 (2016) 31–36. https://doi.org/10.1016/j.fjps.2016.03.001.

[4] T.A. Wani, G. Suresh, Plant-Mediated Green Synthesis of Magnetic Spinel Ferrite Nanoparticles: A Sustainable Trend in Nanotechnology, Advanced Sustainable Systems 6 (2022) 2200035.
https://doi.org/10.1002/adsu.202200035.

[5] N.A.I. Md Ishak, S.K. Kamarudin, S.N. Timmiati, Green synthesis of metal and metal oxide nanoparticles via plant extracts: an overview, Mater. Res. Express 6 (2019) 112004. https://doi.org/10.1088/2053-1591/ab4458.

[6] J. Jeevanandam, Y.S. Chan, M.K. Danquah, Biosynthesis of Metal and Metal Oxide Nanoparticles, ChemBioEng Reviews 3 (2016) 55–67. https://doi.org/10.1002/cben.201500018.

[7] I.A. Shaikh, U.M. Muddapur, Z.K. Bagewadi, S. Chiniwal, M.M. Ghoneim, M.H. Mahnashi, F. Alsaikhan, D. Yaraguppi, F.N. Niyonzima, S.S. More, B.A. Mannasaheb, A. Al Ali, A. Asiri, A.A. Khan, S.M.S. Iqubal, Characterization of Bioactive Compounds from Acacia concinna and Citrus limon, Silver Nanoparticles' Production by A. concinna Extract, and Their Biological Properties., Molecules 27 (2022) 2715.
https://doi.org/10.3390/molecules27092715.

[8] T.A. Bhat, S.A. Wagay, N. Nishat, M.A. Malik, Phyto-Mediated Nanotechnology: A Promising Natural Approach Towards Biomedical Remediations, ChemistrySelect 10 (2025). https://doi.org/10.1002/slct.202502358.

[9] K.K. Ilavenil, V. Senthilkumar, A. Kasthuri, Green synthesis of metal nanoparticles from three medicinal plants: a review of environmental and health applications, Discov Catal 2 (2025). https://doi.org/10.1007/s44344-025-00007-6.

[10] S.A. Ali, A.F. Arafa, H.F. Aly, N.A. Ibrahim, M.O. Kadry, R.M. Abdel-Megeed, M.A. Hamed, A.A. Farghaly, N.S. El Regal, G.I. Fouad, W.K.B. Khalil, E.A. Refaat, DNA damage and genetic aberration induced via different sized silver nanoparticles: Therapeutic approaches of Casimiroa edulis and Glycosmis pentaphylla leaves extracts., J. Food Biochem. 44 (2020). https://doi.org/10.1111/jfbc.13398.

[11] M. Riaz, R. Khalid, M. Afzal, F. Anjum, H. Fatima, S. Zia, G. Rasool, C. Egbuna, A.G. Mtewa, C.Z. Uche, M.A. Aslam, Phytobioactive compounds as therapeutic agents for human diseases: A review, Food Science & Nutrition 11 (2023) 2500–2529. https://doi.org/10.1002/fsn3.3308.

[12] M. Kgatshe, O.S. Aremu, L. Katata-Seru, R. Gopane, Characterization and Antibacterial Activity of Biosynthesized Silver Nanoparticles Using the Ethanolic Extract of *Pelargonium sidoides* DC, Journal of Nanomaterials 2019 (2019) 1–10. https://doi.org/10.1155/2019/3501234.

[13] S. Yasmin, S. Nouren, H.N. Bhatti, D.N. Iqbal, S. Iftikhar, J. Majeed, R. Mustafa, N. Nisar, J. Nisar, A. Nazir, M. Iqbal, H. Rizvi, Green synthesis, characterization and photocatalytic applications of silver nanoparticles using *Diospyros lotus*, Green Processing and Synthesis 9 (2020) 87–96. https://doi.org/10.1515/gps-2020-0010.

[14] F. Mohammadi, M. Yousefi, R. Ghahremanzadeh, Green synthesis, characterization and antimicrobial activity of silver nanoparticles (AgNPs) using leaves and stems extract of some plants, Adv. J. Chem. A 2 (2019) 266–275. https://doi.org/10.33945/sami/ajca.2019.4.1.
[15] S.M. Amini, S. Shahroodian, Antibacterial activity of silver and gold nanoparticles that have been synthesized by curcumin, Inorganic and Nano-Metal Chemistry 55 (2024) 520–526.
https://doi.org/10.1080/24701556.2024.2352352.
[16] Y. Junejo, M. Safdar, M. Ozaslan, Synthesis of Silver Nanoparticles and Their Applications: Review, EPHELS 14 (2024) 22–48. https://doi.org/10.55549/ephels.126.
[17] A. Sobczak-Kupiec, D. Malina, Z. Wzorek, M. Zimowska, Influence of silver nitrate concentration on the properties of silver nanoparticles, Micro Nano Lett. 6 (2011) 656–660. https://doi.org/10.1049/mnl.2011.0152.
[18] B. Venkataesan Kumari, R. Mani, B.R. Asokan, K. Balakrishnan, A. Ramasamy, R. Parthasarathi, C. Kandasamy, R. Govindaraj, N. Vijayakumar, S. Vijayakumar, Green Synthesised Silver Nanoparticles Using Anoectochilus elatus Bark Extract: Characterisation and Evaluation of Antioxidant, Anti-Inflammatory, Antidiabetic, and Antimicrobial Activities, J. Compos. Sci. 7 (2023) 453. https://doi.org/10.3390/jcs7110453.
[19] E. Dilipan, P. Sivaperumal, K. Kamala, M. Ramachandran, P. Vivekanandhan, Green synthesis of silver nanoparticles using seagrass Cymodocea serrulata (R.Br.) Asch. & Magnus, characterization, and evaluation of anticancer, antioxidant, and antiglycemic index., Biotech and App Biochem 70 (2023) 1346–1356. https://doi.org/10.1002/bab.2444.
[20] D. Nayak, S. Ashe, P.R. Rauta, B. Nayak, Biosynthesis, characterisation and antimicrobial activity of silver nanoparticles using Hibiscus rosa-sinensis petals extracts., IET Nanobiotechnology 9 (2015) 288–293. https://doi.org/10.1049/iet-nbt.2014.0047.
[21] M. Azizi, S. Sedaghat, K. Tahvildari, P. Derakhshi, A. Ghaemi, Synthesis of silver nanoparticles using Peganum harmala extract as a green route, Green Chemistry Letters and Reviews 10 (2017) 420–427.
https://doi.org/10.1080/17518253.2017.1395081.
[22] S. Behboodi, F. Baghbani-Arani, S. Abdalan, S.A. Sadat Shandiz, Green Engineered Biomolecule-Capped Silver Nanoparticles Fabricated from Cichorium intybus Extract: In Vitro Assessment on Apoptosis Properties Toward Human Breast Cancer (MCF-7) Cells., Biol Trace Elem Res 187 (2018) 392–402. https://doi.org/10.1007/s12011-018-1392-0.
[23] P. Das, G.J. Ashraf, T. Baishya, T.K. Dua, P. Paul, G. Nandi, A. Dutta, D. Limbu, A. Kumar, M.D. Adhikari, S. Dewanjee, R. Sahu, Formulation of silver nanoparticles using Duabanga grandiflora bark extract and evaluation of their versatile therapeutic applications., Bioprocess Biosyst Eng 47 (2024) 1139–1150.
https://doi.org/10.1007/s00449-024-02975-9.
[24] A. Akintola, B. Kehinde, P. Ayoola, A. Adewoyin, O. Adedosu, J. Ajayi, S. Ogunsona, Antioxidant properties of silver nanoparticles biosynthesized from methanolic bark extract of Blighia sapida, IOP Conf. Ser.: Mater. Sci. Eng. 805 (2020) 012004. https://doi.org/10.1088/1757-899x/805/1/012004.
[25] H. Li, X. Ma, J. Dong, W. Qian, Development of Methodology Based on the Formation Process of Gold Nanoshells for Detecting Hydrogen Peroxide Scavenging Activity, Anal. Chem. 81 (2009) 8916–8922.
https://doi.org/10.1021/ac901534b.
[26] A. Mitra, I.G. Tamil, B. Dineshkumar, M. Nandhakumar, M. Senthilkumar, In vitro study on α-amylase inhibitory activity of an Indian medicinal plant, Phyllanthus amarus, Indian J Pharmacol 42 (2010) 280.
https://doi.org/10.4103/0253-7613.70107.
[27] V.G. Zetic, V. Stehlik-Tomas, S. Grba, L. Lutilsky, D. Kozlek, Chromium uptake bySaccharomyces cerevisiae and isolation of glucose tolerance factor from yeast biomass, J Biosci 26 (2001) 217–223.
https://doi.org/10.1007/bf02703645.
[28] S. Ahmadian, J. Barar, A.A. Saei, M.A.A. Fakhree, Y. Omidi, Cellular Toxicity of Nanogenomedicine in MCF-7 Cell Line: MTT assay, JoVE 49 (2009). https://doi.org/10.3791/1191.
[29] M. Ishiyama, H. Tominaga, M. Shiga, K. Sasamoto, Y. Ohkura, K. Ueno, A combined assay of cell viability and in vitro cytotoxicity with a highly water-soluble tetrazolium salt, neutral red and crystal violet., Biol. Pharm. Bull. 19 (1996) 1518–1520. https://doi.org/10.1248/bpb.19.1518.
[30] K. Halkai, J. Mudda, V. Shivanna, V. Patil, V. Rathod, R. Halkai, Cytotoxicity evaluation of fungal-derived silver nanoparticles on human gingival fibroblast cell line: An in vitro study., J Conserv Dent 22 (2019) 160. https://doi.org/10.4103/jcd.jcd_518_18.
[31] G. Cory, Scratch-Wound Assay, in: Humana, 2011: pp. 25–30. https://doi.org/10.1007/978-1-61779-207-6_2.
[32] J. Pijuan, C. Barceló, D.F. Moreno, O. Maiques, P. Sisó, R.M. Marti, A. Macià, A. Panosa, In vitro Cell Migration, Invasion, and Adhesion Assays: From Cell Imaging to Data Analysis, Front. Cell Dev. Biol. 7 (2019). https://doi.org/10.3389/fcell.2019.00107.
[33] S. Rauf, H. Hameed, M. Tariq, A. Afareen, S. Gulfaraz, N.A. Alkubaisi, M.S. Elshikh, Phytochemical-Mediated Synthesis and Characterization of Silver Nanoparticles Using Mirabilis jalapa Bark Extract and Their Antibacterial., Microscopy Res & Technique 88 (2025) 1795–1805. https://doi.org/10.1002/jemt.24801.

[34] M. Moond, S. Singh, S. Sangwan, S. Rani, A. Beniwal, J. Rani, A. Kumari, I. Rani, P. Devi, Phytofabrication of Silver Nanoparticles Using Trigonella foenum-graceum L. Bark and Evaluation of Its Antimicrobial and Antioxidant Activities, IJMS 24 (2023) 3480. https://doi.org/10.3390/ijms24043480.
[35] S. Bhakya, S. Muthukrishnan, M. Sukumaran, M. Muthukumar, Biogenic synthesis of silver nanoparticles and their antioxidant and antibacterial activity, Appl Nanosci 6 (2015) 755–766. https://doi.org/10.1007/s13204-015-0473-z.
[36] R. Santhoshkumar, A. Hima Parvathy, E.V. Soniya, Phytosynthesis of silver nanoparticles from aqueous bark extracts of Piper colubrinum: characterisation and catalytic activity, Journal of Experimental Nanoscience 16 (2021) 294–308. https://doi.org/10.1080/17458080.2021.1970140.
[37] R. Golabiazar, K.I. Othman, K.M. Khalid, D.H. Maruf, S.M. Aulla, P.A. Yusif, Green Synthesis, Characterization, and Investigation Antibacterial Activity of Silver Nanoparticles Using Pistacia atlantica Bark Extract, BioNanoSci. 9 (2019) 323–333. https://doi.org/10.1007/s12668-019-0606-z.
[38] R. Rani, D. Sharma, M. Chaturvedi, J.P. Yadav, Green synthesis of silver nanoparticles using Tridax procumbens: their characterization, antioxidant and antibacterial activity against MDR and reference bacterial strains, Chem. Pap. 74 (2019) 1817–1830. https://doi.org/10.1007/s11696-019-01028-w.
[39] D. Jini, S. Sharmila, A. Anitha, M. Pandian, R.M.H. Rajapaksha, In vitro and in silico studies of silver nanoparticles (AgNPs) from Allium sativum against diabetes, Sci Rep 12 (2022). https://doi.org/10.1038/s41598-022-24818-x.
[40] S. Gurunathan, J.W. Han, V. Eppakayala, M. Jeyaraj, J.-H. Kim, Cytotoxicity of Biologically Synthesized Silver Nanoparticles in MDA-MB-231 Human Breast Cancer Cells, BioMed Research International 2013 (2013) 1–10. https://doi.org/10.1155/2013/535796.
[41] D. Veeragoni, S. Deshpande, H.K. Rachamalla, A. Ande, S. Misra, S.R. Mutheneni, In Vitro and In Vivo Anticancer and Genotoxicity Profiles of Green Synthesized and Chemically Synthesized Silver Nanoparticles., ACS Appl. Bio Mater. 5 (2022) 2324–2339. https://doi.org/10.1021/acsabm.2c00149.
[42] M. Muhamad, N. Ab.Rahim, W.A. Wan Omar, N.N.S. Nik Mohamed Kamal, Cytotoxicity and Genotoxicity of Biogenic Silver Nanoparticles in A549 and BEAS-2B Cell Lines, Bioinorganic Chemistry and Applications 2022 (2022) 1–22. https://doi.org/10.1155/2022/8546079.
[43] M. Składanowski, P. Golinska, K. Rudnicka, H. Dahm, M. Rai, Evaluation of cytotoxicity, immune compatibility and antibacterial activity of biogenic silver nanoparticles, Med Microbiol Immunol 205 (2016) 603–613. https://doi.org/10.1007/s00430-016-0477-7.
[44] M. Fahim, A. Shahzaib, N. Nishat, A. Jahan, T.A. Bhat, A. Inam, Green synthesis of silver nanoparticles: A comprehensive review of methods, influencing factors, and applications, JCIS Open 16 (2024) 100125. https://doi.org/10.1016/j.jciso.2024.100125.
[45] B. Javed, M. Ikram, F. Farooq, T. Sultana, Z.-U.-R. Mashwani, N.I. Raja, Biogenesis of silver nanoparticles to treat cancer, diabetes, and microbial infections: a mechanistic overview., Appl Microbiol Biotechnol 105 (2021) 2261–2275. https://doi.org/10.1007/s00253-021-11171-8.
[46] A.R. Sharma, G. Sharma, S. Nath, S.-S. Lee, Screening the phytochemicals in Perilla leaves and phytosynthesis of bioactive silver nanoparticles for potential antioxidant and wound-healing application, Green Processing and Synthesis 13 (2024). https://doi.org/10.1515/gps-2024-0050.